Journal of
Materials Chemistry C

Materials for optical, magnetic and electronic devices

Accepted Manuscript

This article can be cited before page numbers have been issued, to do this please use: M. S. Lassoued, L. Bi, Z. Wu, G. Zhou and Y. Zheng, *J. Mater. Chem. C*, 2020, DOI: 10.1039/D0TC01017K.

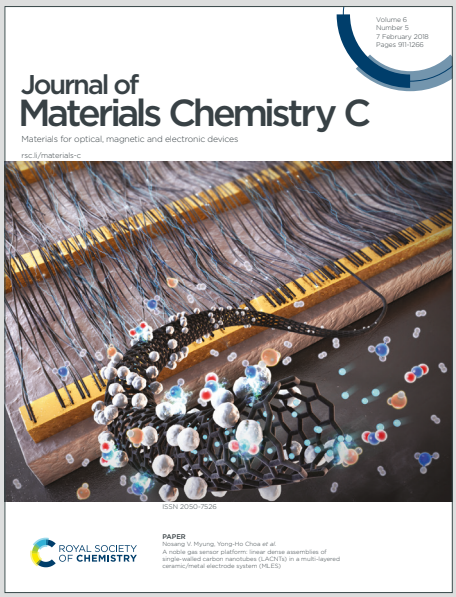

ROYAL SOCIETY OF CHEMISTRY

rsc.li/materials-c

View Article Online
DOI: 10.1039/D0TC01017K

COMMUNICATION

Piperidine Switches on Direct Band Gaps of Ag(I)/Bi(III) Bimetallic Iodide Double Perovskites

Received 00th January 20xx,
Accepted 00th January 20xx

DOI: 10.1039/x0xx00000x

Mohamed Saber Lassoued,[a] Le-Yu Bi,[a] Zhaoxin Wu,[b,c] Guijiang Zhou,[d] and Yan-Zhen Zheng*[a]

The environmental toxity of lead may eventually hamper the wide application of hybrid perovsite material based solar cells despite their excellent power conversion efficiency. Here we use silver(I) and bismuth(III) to replace lead(II) and obtain two two-dimensional (2D) iodide-based double perovskites, $(AMP)_4[BiAgI_8]_2.H_2O$ 1 and $(APP)_4[BiAgI_8].H_2O$ 2, where AMP = 4-aminomethylpiperidine and APP = 4-aminopiperidine. Comparing to our previously reported 1,4-cyclohexanediamine based compound $(C_6H_{16}N_2)_2[BiAgI_8].H_2O$ with indirect band gap, these two new 2D Ag-Bi double perovskites show direct band gaps ~ 2.00 eV due to the less distorted $[AgI_6]$ coordination geometry. Moreover, the photo-current response experiments show more than 50 nA difference between Ilight and Idark for both compounds, indicating the potential application for light harvesting. 1 and 2 are also stable under heat and moisture. They show high proton conductivity (~10^{-4} S cm^{-1}) at 95 °C and 90% RH. Thus, this work provides a new road for design stable lead-free bimetallic iodide double perovskites with direct band gaps.

a Dr. M. S. Lassoued, L.-Y. Bi, Prof. Dr. Y.-Z. Zheng
Frontier Institute of Science and Technology (FIST), State Key Laboratory for Mechanical Behavior of Materials, MOE Key Laboratory for Nonequilibrium Synthesis and Modulation of Condensed Matter, Xi'an Key Laboratory of Sustainable Energy and Materials Chemistry, and School of Science, Xi'an Jiaotong University, Xi'an 710049, China.
E-mail: zheng.yanzhen@xjtu.edu.cn.

b,c Prof. Dr. Zhaoxin Wu
Key Laboratory of Photonics Technology for Information, Key Laboratory for Physical Electronics and Devices of the Ministry of Education, Department of Electronic Science and Technology, School of Electronic and Information Engineering, Xi'an Jiaotong University, Xi'an, China d.Collaborative Innovation Center of Extreme Optics, Shanxi University, Taiyuan 030006, China

d Prof. Dr. Guijiang Zhou
Ministry of Education Key Laboratory for Nonequilibrium Synthesis and Modulation of Condensed Matter and Department of Chemistry, Faculty of Science, Xi'an Jiao Tong University, Xi'an 710049, P. R. China
Supporting information for this article is given via a link at the end of the document

Though the power conversion efficiency (PCE) of the solar cells based on the prototype hybrid perovskite material -- $(MA)PbX_3$ (MA = methylammonium) -- has ascended from 3.6% to 25.2% within ten years, [1] the material still suffers poor air stability and high toxicity of lead.[2-4] To address the long-term stability issue for practical application, in literature, scientists have been paid much interest to improve stability of perovskite compounds among them Wu et al showed that alloying Ba into $MAPbI_3$ perovskites is beneficial of the stability and have been emerged as an attractive material for photovoltaics applications.[5] Recently Zheng et al showed that two dimensional (2D) inorganic/organic perovskites present as a new road to obtain stable compound with very promising properties in optoelectronic devices.[6]

In terms of the toxicity of lead, it is almost impossible to use environmentally–friendly divalent metal ions to replace Pb^{2+}, because, for instance, the ion sizes of Mg^{2+} and Ba^{2+} are too large to form a stable perovskite structure; the band gaps of Ca^{2+} and Sr^{2+} compounds are too large due to the lack of lone pairs of electrons; and the Sn^{2+} is simply oxidized into Sn^{4+}.[7-9] Thus, the trivalent bismuth(III) which has $6s^2$ lone pair electrons and stable valence has become the most promising candidate,[10,11] but the charge is not balanced if a perovskite structure is targeted. An effective method to solve this problem is to combine a monovalent cation such as K(I), Na(I), Ag(I) and Cu(I), which can balance the surplus charge of trivalent metal during the formation of the lead-free organic-inorganic hybrid structures. In this context bimetallic double perovskites are very promising for its high stability and attractive optoelectronic properties.[12-15]

However, the fabrication of bimetallic hybrid perovskite is challenging. Until a few years ago, there started the incorporation of trivalent cation (M^{III}) and monovalent (M^{I}) into organic/inorganic hybrid or inorganic material. In 2016, McClure et al have synthesized the first inorganic bimetallic lead free double perovskite Cs_2AgBiX_6 (X = Br, Cl) with band gap of 2.19 eV for X = Br and 2.77 eV for X=Cl.[16] $Cs_2AgBiBr_6$ have been also reported by Karunadasa et al but with the band gap of 1.95 eV and long photoluminescence life time of ca. 660 ns.[17] Later, Zhang et al also exploited the strategy of cation transmutation to transform two divalent Pb^{+2} ions into one monovalent M^+ and

DOI: 10.1039/D0TC01017K

one trivalent M^{3+} ions, synthesizing a novel class of quaternary halides within double perovskites (elpasolites) like $Cs_2InBiCl_6$ and Cs_2AgSbI_6 etc. They further identified eleven non-toxic perovskites as promising absorbers to replace $APbX^{VII}_3$.[18] In 2018 Karunadasa et al first synthesized two Ag-Bi bromide hybrid double perovskites, namely $(BA)_4AgBiBr_8$ and $(BA)_2AgBiBr_7$, [BA = $CH_3(CH_2)_3NH_3^+$] with widened band gaps.[19]

Compared to bromide and chloride, metal iodides have been less studied for the construction of hybrid material. In literature, only one two-dimensional (2D) Ag(I)-Bi(III) iodide double perovskite templated by a layer of bifunctionalized oligothiophene cations has been reported recently.[20] and several months ago, our group reported a second 2D perovskite compound $(C_6H_{16}N_2)_2[BiAgI_8].H_2O$ (**AgBiI**) [$C_6H_{14}N_2$ = 1,4-cyclohexane-diamine].[21] We found that **AgBiI** exhibits indirect band gap. Here we find that the amines and structural distortions energetically play important role to differentiate between direct and indirect band gaps. The two new compounds, namely $(AMP)_4[BiAgI_8]_2.H_2O$ **1** and $(APP)_4[BiAgI_8].H_2O$ **2**, where AMP = 4-aminomethylpiperidine and APP = 4-aminopiperidine, show direct band gaps of ~2.00 eV, which have been corroborated by UV absorption, photoluminescence and *ab-inito* calculation. In addition to the high solubility and film processable nature, **1** and **2** show significant stability against moisture and temperature. This can be proved by the proton conducting properties of **1** and **2** at high temperature and high humidity. A conductivity of ~10^{-4} S cm^{-1} is recorded at 95 °C and 90% RH.

Single crystals of **1** and **2** were grown through hydrothermal method of stoichiometric amounts of AgI, BiI_3, and AMP or APP in a concentrated hydroiodic acid solution at 120 °C for three days (see "Materials and sample preparation" in the SI for more details). Compound **1** crystallizes in the monoclinic space group $C2_1/c$ (see **Table S1**, supporting information). The inorganic moiety of **1** forms a $[AgBiI_8]_n^{4n-}$ double perovskite structure, which is separated by the organic $[(NH_3^+\text{-}CH_2\text{-}C_5NH_{10})_2]^{4+}$ cations (**Figure 1a** and **S1a**). The $[AgBiI_8]_n^{4n-}$ layer was assembled through the Bi-I-Ag bridges to form vertex-sharing $[BiI_6]$ and $[AgI_6]$ octahedron (**Figure 2a**). The bond distances of Bi-I range from 2.9849(10) Å to 3.2118(13) Å, and the I_{eq}-Bi-I_{eq} (eq refer to equatorial) and I_{ax}-Bi-I_{ax} (ax refer to axial) angles range from 86.85(3)° to 93.35(4)° and from 173.657(18)° to 176.643(19)°, respectively, indicating slightly distorted from the ideal octahedron. The bond distances of Ag-I range from 2.667(11) Å to 3.786(10) Å, and the I_{eq}-Ag-I_{eq} and I_{ax}-Agi-I_{ax} angles range from 87.76(3)° to 93.41(3)° and from 170.24(6)° to 180°, respectively. These values are in good agreement with similar compounds.[20, 21]

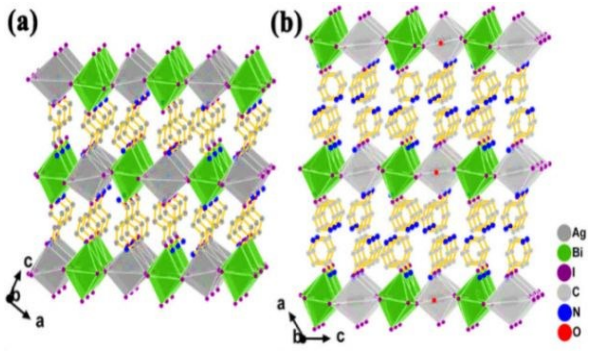

Figure 1. Crystal structures of **1** (a) and **2** (b). Colors are indicated on the right panel and the same applied to the following picture.

Single crystal X-ray diffraction analysis reveals that **2** crystallizes in the space group C2/c (**Table S1**, **ESI†**). The silver atom is distorted over three sites with occupancies 0.1 : 0.8 : 0.1 by symmetries (**Figure S1b**, **ESI†**). As shown in **Figure 1b** and **Figure 2b**, the crystal structure forms typical organic-inorganic 2D double perovskite architecture by vertex sharing octahedral of Bi^{3+} and Ag^+ cations. For the inorganic moieties of **2**, each Bi^{3+} and Ag^+ ion is surrounded by six I atoms forming a distorted octahedron configuration with Bi-I and Ag-I bond lengths varying from 3.0727(8) Å to 3.1054(10) Å and from 2.6928(12) Å to 3.229(9) Å, respectively. These distances are closer to the sum of the ionic radius of bismuth/silver and iodine atoms (ri = 1.03 + 2.2 = 3.23 Å/ri = 1.15 + 2.2 = 3.35 Å) rather than to that of their covalent radius (re = 1.48 + 1.39 = 2.87 Å/re = 1.45 + 1.39 = 2.84 Å) indicating that these bond have an ionic and slightly distorted character of the BiI_6 and AgI_6 octahedron.

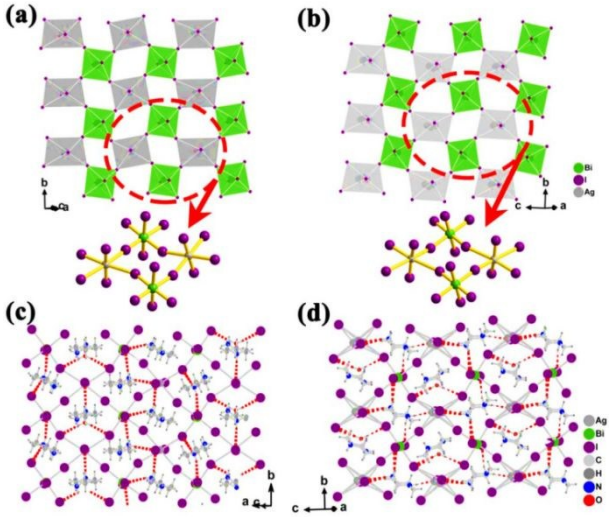

Figure 2. Inorganic structure of the 2D $[AgBiI_8]^{4-}$ of **1** (a) and **2** (b). Perspective view of the hydrogen bonding network in **1** (c) and **2** (d) (the red dotted lines represent hydrogen bonds).

Interestingly, 4-aminomethylpiperidine and 4-aminopiperidine play important role to construct 2D perovskite due to their distorted geometry which can support firmly inorganic layer. Indeed, AMP and APP exhibits a regular spatial configuration with normal C-C and C-N distances ranging from 1.493(12) Å to 1.538(13) Å, C-C-C and C-C-N angles ranging between 108.2(8)° and 113.5(8)° (see **Table S2** and **S3**, **ESI†**). Moreover, **1** and **2** exhibit many intermolecular hydrogen bonding contacts between the cationic ($[(NH_3^+\text{-}CH_2\text{-}C_5NH_{10})_2]^{4+}$ or $[(C_6H_{12}N_2)_2]^{2+}$, H_2O and $[AgBiI_8]^{4-}$ anions of the type N-H···I, O-H···N and O-H···I reported in **Figure 2c** and **2d**, **Table S4** and **S5** in the supporting information.

The distortion degree of BiI_6 and AgI_6 octahedron in **1** and **2** (Δd and σ^2) can be quantitatively estimated following equations [22,23] and compared to our reported **AgBiI** perovskite.[21]

$$\Delta d = (1/6)\sum [dn\text{-}d/d]^2 \quad (1)$$

$$\sigma^2 = \sum (\Theta i\text{-}90)^2/11 \quad (2)$$

View Article Online
DOI: 10.1039/D0TC01017K

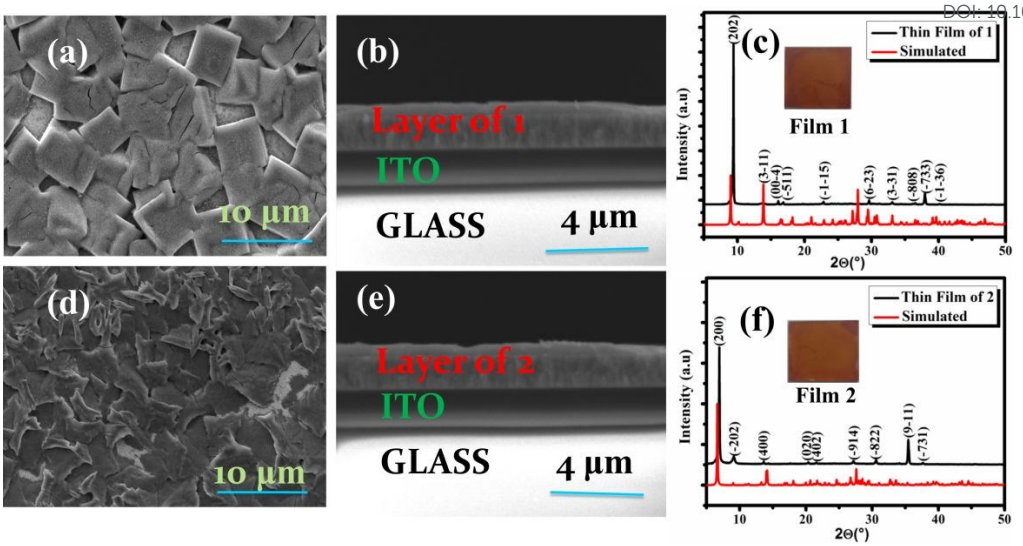

Figure 3. (a) Topographical SEM images of the thin film made from **1**. (b) Cross-sectional SEM image of thin film made from **1**. (c) XRD patterns the thin film made from **1**. Inset: photographs of the film. (d) Topographical SEM images of the thin film made from **2**. (e) Cross-sectional SEM image of thin film made from **2**. (f) XRD patterns of the thin film made from **2**. Inset: photographs the films.

Where "d" is the average distance of the six M-I (M = Bi or Ag) bonds forming the octahedron and "dn" refers to the six individual Bi-I or Ag-I bond length. Similarly, the bond angle variance (Eq2, where "Θi" is the individual X-M-X angle) 90°, referring to the angle deviation of the non-distorted structure, can be also calculated.

Table 1 Distortion degree of metal coordination geometries for **1**, **2** and **AgBiI**.

	1			***2***		***AgBiI***	
	[BiI_6]	*[Ag_1I_6]*	*[Ag_2I_6]*	*[BiI_6]*	*[AgI_6]*	*[BiI_6]*	*[AgI_6]*
$\Delta d/10^{-3}$	*0.14*	*1.46*	*3.3*	*0.004*	*2.48*	*0.01*	*5.1*
$\sigma^2(°)$	*136.7*	*151.1*	*134*	*147.49*	*129.7*	*138.6*	*108.9*

From **Table 1** we can see all the [AgI_6] octahedra are distorted, in particular for **AgBiI** in that their band distances and angles are strongly deviated from the ideal values as demonstrated by the distortion parameters Δd and σ^2 which present the largest Δd and the smallest σ^2 parameters.

The PXRD patterns of **1** and **2** match perfectly well with the simulated one based on the single-crystal structure, indicating a pure phase of our powder samples (**Figure S2 (a, b), ESI†**).

Interestingly, both **1** and **2** are highly soluble in DMF that 1 ml DMF can dissolve 1 g of solids. By spin coating method, o.4 g/ml DMF solution of **1** and **2** deposited on ITO glass followed by annealing on a hot plate at 70 °C for 10 minutes and cooled to room temperature. We got a smooth, uniform with less pin-hole thin film of **1** and **2** (**Figure 3 (a, d)**) with grain size of 4 µm and 3 µm respectively. The thickness of films was obtained through the cross section images in **Figure 3b** and **3e** revealed that the film had the thickness of 1 µm and 1.2 µm of **1** and **2**, respectively which are in good agreement with other films perovskites.[24,25] We successfully prepared uniform thin films to avoid the pinholes and to ensure the interconnectivity between the crystallites with ~1 µm thickness to absorb high light capacity. **Figures 3c** and **3f** show that XRD patterns films of **1** and **2** are in good agreement compared with the patterns generated from the single crystal data indicating the phase purity of our thin films compound. An important point is cited here that for the most studied halide perovskites, the inorganic layers highly grow parallel to the substrate surface.[26] In this paper, the XRD patterns for films **1** and **2** show a principal (202) and (200) reflection respectively which means the vertical growth of the compound on the substrate.

Diffuse reflectance spectrum was determined with polycrystalline powders at room temperature and converted to absorbance spectrum by Kubelka-Munk transformation. [27, 28] Compounds **1** and **2** have absorption cutoff wavelengths of 620 nm (2.00 eV) and 604 nm (2.05 eV), respectively. These values are in good agreement with those observed in similar compounds. [29, 30]

The Tauc plots obtained from their absorption spectra by assuming a direct band gap agree well with absorbance values, which show Eg of 2.07 eV and 2.12 eV for **1** and **2**, respectively (**Figure 4a**).

The absorption spectra of the thin films **1** and **2** at 298 K were also determined to be 588 nm (2.11 eV) and 566 nm (2.19 eV), respectively (**Figure S3**, **ESI†**), both slightly higher than those of the powder samples, which may due to the scattering according to the Mie theory.[31-33] We need to mention that the presence of such narrow band indicates a high excitonic binding energy produced by the dielectric mismatch between organic and inorganic entities.

We have analyzed the nature of the electronic states in valence band maximum (VBM) and the conduction band minimum (CBM) near the band gap, using a projection of the total density of states (**Figures 4b** and **S4a-d**, **ESI†**). The VB is mainly contributed by I-p and Ag-d orbitals while the electronic states at the CB are predominantly contributed by Bi-p, I-p and Ag-s orbitals. This indicates that the optical properties of **1** near its band gap originate from the inorganic $[AgBiI_8]^{4-}$ components.

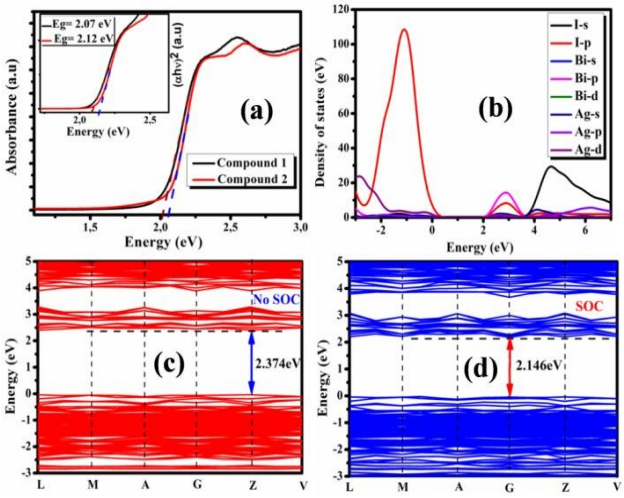

Figure 4. (a) Absorption spectra for the powder 1 and 2. The upper inset shows the Tauc Plot for a direct band gap semiconductor. (b) Partial density of states (PDOS) of inorganic part of 1. (c) The band structure of 1 without SOC. (d) The band structure of 1 with SOC.

Without SOC, both VBM and the CBM for **1** are located at Z point which should be reminiscent of the direct feature of its band gap (**Figure 4c**). The calculated energy of **1** is 2.37 eV which is slightly larger than the value of the direct band gap obtained from the UV−Vis absorption spectrum (2.07 eV).[34-37] When spin-orbital coupling (SOC) is taken into account, the band gap is reduced to 2.14 eV, and the band curvatures changed to near conduction band G (**Figure 4d**). Note that a direct band gap was also observed for the 2D lead free perovskite $(BA)_4AgBiBr_8$ but at 2.85 eV.[19]

However, our previous reported compound (**AgBiI**) has indirect band gap (**Figure S4e**, **ESI†**), **1** and **2** have direct gap energy. To understand this difference, we have analyzed the geometrical distortion of the $[AgI_6]$ octahedron in **AgBiI**, **1** and **2**, For **AgBiI**, the $[AgI_6]$ octahedron is significantly distorted (see **Table 1**), forming a shorter Ag-I bond (2.684 Å) in the axial position and a much longer Ag-I bond ranged between 2.970 Å and 4.324 Å in the equatorial plane. For **1** the equatorial Ag-I distance is much shorter, ranging from 3.381 Å to 3.786 Å and the axial little longer about 2.732 Å. For **2**, this is similar, where the Ag-I_{eq} distance grouped between 3.212 Å and 3.229 Å. Indeed this distortion in $[AgI_6]$ for **AgBiI** compound induces changes in orbital "d" at the Ag site which alters the valence band (VB) dispersion. Therefore, the structural distortions energetically play important role to differentiate the direct and indirect transitions. This finding means Ag-4d states is responsible for the band gap structure, where the long Ag-I_{ax} bonds stabilize the antibonding VBM states of Ag dz^2 character and the short Ag-I_{eq} bonds destabilize those of Ag dx^2-y^2 character (both situation are favorable for direct band gap).

Under UV-radiation at 450 nm, Compounds **1** and **2** exhibit weak emission bands centering at 605 nm and 587 nm with CIE chromaticity coordinates of (0.44, 0.52) and (0.49, 0.48), respectively, which is derive from spatial localization/separation of photoexcited holes and electrons in the vicinity of Ag and Bi, respectively (**Figure S5a** and **S5b**, **ESI†**).[21, 38] The correlated color temperatures (CCT) are 3676 K and 2756 K for **1** and **2**, respectively, corresponding to the yellowish-white (warm) light for indoor illumination. The broadband emission of **1** and **2** enables it to have a color rendering index (CRI) of 40 and 58 respectively. Furthermore, the average life times were recorded with double exponential according to $\tau = \tau 1\alpha 1 + \tau 2\alpha 2$ with $\tau 1$ is the fastest decay process was related to the radiative recombination of excitons, $\tau 2$ is the slowest decay process corresponded to the trap states due to the perovskite crystal structure, **a1** and **a2** refer to the occupancy of each decay time. The average life time are calculated to be 5.97 ns and 6.23 ns for **1** and **2** respectively (**Figure S5c**, **ESI†**). Thus, these two compounds show longer average life time emission compared to $MAPbI_3$ (τ**avr** = 2.85 ns) and other reported perovskite compounds (**Figure 5** and **Table S6**, **ESI†**).[39-42] This result can be assigned to the decrease of the nonradiative recombination in the layered crystal structure.

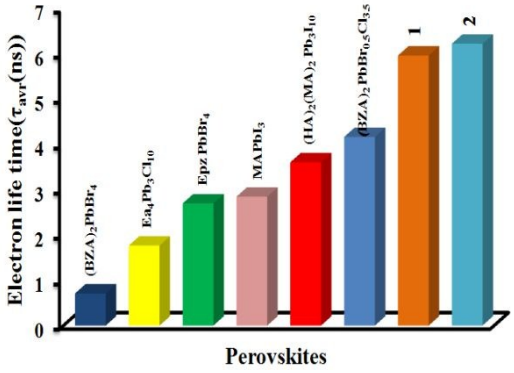

Figure 5. The fluorescence average decay time spectrum of **1**, **2** and the reported ones.

To reveal the possibility for optoelectronic application, we measured the photoconductivity of the two compounds using pressed pellet samples under 350 W Xenon lamp irradiation. As shown in **Figure S6a** and **S6b** at a positive bias voltage of 3 V, the photocurrent is enhanced from 5.64 nA (dark) to 79.31 nA (light) for **1** and from 2.80 nA (dark) to 56.01 nA (light) for **2**, which shows an obvious switch of 14.06 nA and 20 nA (on/off) for **1** and **2**, respectively (**Table 2**). A periodically turning the light on and off has been recorded for **1** and **2** (**Figure S6c** and **S6d**, **ESI†**), indicating the reproducibility and superior stability of **1** and **2**. Note that these two perovskites showed an enhanced photocurrent response compared to our reported **AgBiI** compound, which may also due to the direct band gap nature. Besides to their interesting photodetection properties, $(AMP)_4[BiAgI_8]_2.H_2O$ and $(APP)_4[BiAgI_8].H_2O$ may exhibit promising thermal conductivity measurement as shown by Wu et al whose synthesized 0D Lead-Free Hybrid Crystal $[Mn(C_2H_6OS)_6]I_4$ with an ultralow thermal conductivity of 0.15 ± 0.01 W m^{-1} K^{-1} at room temperature, which is among the lowest values reported for organic–inorganic hybrid materials.[43] Measuring thermal conductivity is one of our next future research goals in order to improve our 2D double perovskite physical properties.

Table 2 Photoelectric response for **1** and **2** at ± 3 V under 350 W Xenon lamp irradiation.

Compd	I_{light}(+) (nA)	I_{dark}(+) (nA)	I_{light}/I_{dark}(+)	I_{light}(-) (nA)	I_{dark}(-) (nA)	I_{light}/I_{dark}(-)
1	79.31	5.64	14.06	-78.87	-6.4	12.32
2	56.01	2.80	20	-55.71	-2.78	20.03

The presence of protonated piperidine amines and water molecule as proton carriers and hydrogen-bonding liaisons as proton-conducting pathways make **1** and **2** appropriate to be used in proton-conducting solid materials. Usually, the proton-conducting property of materials is mainly influenced by relative temperature and humidity. Herein, variable humidity (30%-90%, relative humidity (RH)) dependent proton conductivity has been conducted through a pressed pellet and measured by alternating-Current spectroscopy at 368 K. Amazingly, as shown in **Figure 6a-d**, the proton conductivities of compound **1** increase from 1.06×10^{-5} S cm^{-1} to 2.27×10^{-4} S cm^{-1} along with increasing RH (30-90%), while under the same measurements, proton conductivities of compound **2** augment from 7.19×10^{-6} S cm^{-1} to 2.09×10^{-4} S cm^{-1}.

From those results mentioned above, it is suggested that water molecules are the main source of proton carriers in the crystalline solid to improve the proton conductivities of the compounds higher RH condition was applied, while the high temperature provides activation energy to reach the ionization into H^+ which results in higher proton conductivities.[44,45] Interestingly, both compounds show high stability during the measurement. The proton conductivity of **1** is better of **2** under the same conditions probably due to the bond strength between water molecules, H^+ and the metal cations, and to the number of hydrogen bonding formed in compound **1** is more than that in **2**. These results are very interesting comparably to those of the hybrid organic/inorganic compound and MOF proton conductors as shown in **Table S7** in the supporting information.

Not only stable under high humidity as indicated above for both compounds thermogravimetric analysis (TGA) reveals that both **1** and **2** are stable up to 290 °C and 285 °C, respectively (**Figure S7**, **ESI†**). To further reveal the stability of these two compounds under moisture both as prepared powders and thin films of **1** and **2** were stored in the dark at 55% humidity for 7 and 30 days respectively. As shown in **Figure S8** and **S9** in the supporting information, we find XRD powders and thin films of **1** and **2** are almost the same as those of the as-prepared sample and there were no extra peak related to the degradation products appears. Hence, these two materials are very stable and robust to moisture and heat.

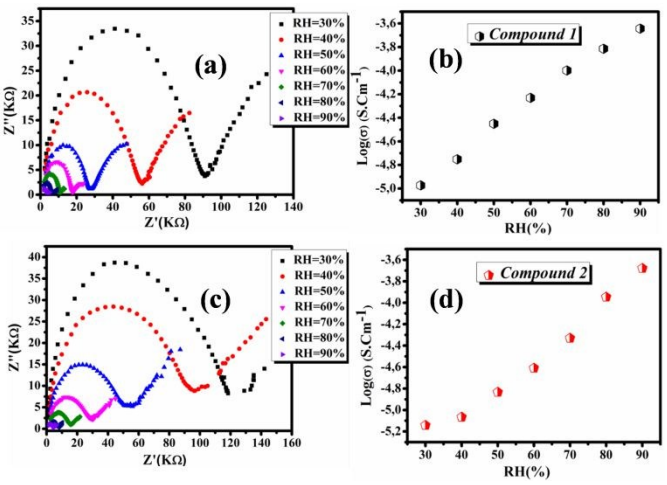

Figure 6. Temperature-dependent Nyquist plots for **1** (a) and **2** (c) measured at 95°C. Proton conduction of compounds **1** (b) and **2** (d) measured at 30%, 40%, 50%, 60%, 70%, 80% and 90% RH at 95 °C

Conclusions

In summary, by using piperidine based amines as templates, we successfully switch the indirect band gap of the monolayer silver/bismuth iodine hybrid double perovskites to the direct band gaps, which is mainly due to the reduced distortion of the [AgI_6] octahedron. This finding also corroborates the Ag-4d orbital determines the bang gap structure of the bimetallic double perovskites. Specifically, in these two compounds the elongated Ag-Iax bonds stabilize the antibonding VBM states of Ag dz^2 character, while the shorter Ag-I_{eq} bonds destabilize those of Ag dx^2-y^2 character. Both actions promote the direct band gap features. Moreover, both compounds exhibit strong photocurrent responses when irradiating under Xenon lamp, proving the possibility of their application in optoelectronics and solar cell. In addition, these two compounds show high proton conductivities at high temperature and moisture, indicating they are very stable when exposed to the air, rendering the futuristic application in real world.

Conflicts of interest

There are no conflicts to declare.

Acknowledgements

This work was supported by Shenzhen Science and Technology Program (JCYJ20180306170859634), Natural Science Foundation of China (nos. 21971203 and 21773130), State Key Laboratory for Mechanical Behavior of Materials (20182006), Key Laboratory Construction Program of Xi'an Municipal Bureau of Science and Technology (201805056ZD7CG40), China Postdoctoral Science Foundation (2018M631138), Shaanxi Postdoctoral Science Foundation (2018), Cyrus Chung Ying Tang Foundation and Fundamental Research Funds for Central Universities.

References

1. The National Renewable Energy Laboratory (NREL) Best Research-Cell Record Efficiencies, https://www.nrel.gov/pv/assets/pdfs/best-research-cellefficiencies. 20190703.pdf (accessed 27 August 2019).
2. A. Latini, G. Gigli, A. Ciccioli, Sustainable Energy Fuels., **2017**, 1, 1351-1357.
3. L. Etgar, Energy and Environmental Science., **2018**, 11, 234-242.
4. B. W. Park, S. I. Seok, Advanced Materials., **2019**, 3, 1805337.
5. M-H. Shang, J. Zhang, P. Zhang, Z. Yang, J. Zheng, M. A. Haque, W. Yang, S-H. Wei, and T. Wu, Journal of Physical Chemistry Letters., **2019**, 10, 59-66.
6. L-Y. Bi, T. Hu, M-Q. Li, B-K. Ling, M. S. Lassoued, Y-Q. Hu, Z. Wu, G. Zhou and Y-Z. Zheng., Journal of Material Chemistry A., **2020**, Accepted Manuscript.
7. D. Ray, C. Clark, H. Q. Pham, J. Borycza , R. J. Holmesb , E. S. Aydilb , L. Gagliardi. Journal of Physical Chemistry C., **2018**, 122, 7838-7848.
8. E. S. Parrott, R. L. Milot, T. Stergiopoulos, H. J. Snaith, M. B. Johnston, L. M. Herz, Journal of Physical Chemistry Letters., **2016**, 7, 1321–1326.
9. C. C. Stoumpos, C. D. Malliakas, M. G. Kanatzidis, Inorganic Chemistry., **2013**, 52, 9019 − 9038.
10. Z. Shi, J. Guo, Y. Chen, Q. Li, Y. Pan, H. Zhang, Y. Xia, W. Huang, Advanced Materials., **2017**, 29, 1605005−1605033.

11. M. Leng, Z. Chen, Y. Yang, Z. Li, K. Zeng, K. Li, G. Niu, Y. He, Q. Zhou, J. Tang, Angewandte Chemie International Edition., **2016**, 55, 15012−15016.
12. G. G-Espejo, D. R-Padrón, R. Luque, L. Camacho and G. de Miguel, Nanoscale., **2019**, 11, 16650-16657.
13. H. Q. Pham, R. J. Holmes, E. S. Aydil and L. Gagliardi, Nanoscale., **2019**, 11, 11173-11182.
14. U-G. Jong, C-J. Yu and Y-H. Kye, RSC Advances., **2020**, 10, 201-209.
15. E. Greul, M. L. Petrus, A. Binek, P. Docampo and T. Bein, Journal of Material Chemistry A., **2017**, 5, 19972-19981.
16. E. T. McClure, M. R. Ball, W. Windl, P. M. Woodward, Chemistry of Material., **2016**, 28, 1348-1354.
17. A. H. Slavney, T. Hu, A. M. Lindenberg, and H. I. Karunadasa, Journal of the American Chemical Society., **2016**, 138, 2138-2141.
18. X. Zhao, J. Yang, Y. Fu, D. Yang, Q. Xu, L. Yu, S-H. Wei, and L. Zhang, Journal of the American Chemical Society., **2017**, 139, 2630-2638.
19. B. A. Connor, L. Leppert, M. D. Smith, J. B. Neaton, H. I. Karunadasa, Journal of the American Chemical Society., **2018**, 140, 5235-5240.
20. M. K. Jana, S. M. Janke, D. J. Dirkes, S. Dovletgeldi, C. Liu, X. Qin, K. Gundogdu, W. You, V. Blum, and D. B. Mitzi., Journal of the American Chemical Society., **2019**, 141, 7955-7964.
21. L-Y. Bi, Y-Q. Hu, M-Q. Li, T-L. Hu, H-L. Zhang, X-T. Yin, W-X. Que, M. S. Lassoued, and Y-Z. Zheng, Journal of Material Chemistry A., **2019**, 7, 19662-19667.
22. J. Alonso, M. Martinez-Lope, M. Casais, M. Fernandez-Diaz, Inorganic Chemistry., **2000**, 39, 917−923.
23. K. Robinson, G. V. Gibbs, P. H. Ribbe, Science., **1971**, 172, 567-569.
24. M-H. Jung, Journal of Material Chemistry A., **2019**, 7, 14689-14704.
25. M. Ghasemi, M. Lyu, M. Roknuzzaman, J-Ho. Yun, M. Hao, D. He, Y. Bai, P. Chen, P. V. Bernhardt, K.(Ken) Ostrikov and L. Wang, Journal of Material Chemistry A., **2019**, 7, 20733-20741.
26. D. H. Cao, C. C. Stoumpos, O. K. Farha, J. T. Hupp, and M. G. Kanatzidis, Journal of the American Chemical Society., **2015**, 137, 7843-7850.
27. P. Kubelka, Z. Technical Physics., **1931**, 12, 593-601.
28. J. Tauc, Material Research Bulletin., **1970**, 5, 721−729.
29. P. Cheng, T. Wu, Y. Li, L. Jiang, W. Deng and K. Han, New Journal of Chemistry., **2017**, 41, 9598-9601.
30. W.-X. Chai, L.-M. Wu, J.-Q. Li, L. Chen, Inorganic Chemistry., **2007**, 46, 1042−1044.
31. A P. Prishivalko, Journal of Applied Spectroscopy., **1996**, 63, 675-683.
32. M. Elias, Applied Optics., **2011**, 50, 2464-2473.
33. A. M. Gueli, G. Bonfiglio, S. Pasquale, et al., Color Research & Application., **2017**, 42, 236-243.
34. R. W. Godby, M. Schluter, L. Sham, Physical Review B: Condens. Matter Mater. Phys., **1987**, 36, 6497−6500.
35. C. M. I. Okoye, Journal of Physics: Condensed Matter., **2003**, 15, 5945−5958.
36. R. Terki, G. Bertrand, H. Aourag, Microelectronic Engineering., **2005**, 81, 514−523.
37. M-J. Wang, X-R. Xuan-Rong Chen, Y-B. Tong, G-J. Yuan, X-M. Ren, and J-L. Liu, Inorganic Chemistry., **2017**, 56, 9525-9534.
38. L. Mao, S. M. L. Teicher, C. C. Stoumpos, R. M. Kennard, R. A. DeCrescent, G. Wu, J. A. Schuller, M. L. Chabinyc, A. K. Cheetham, and R. Seshadri, J. Am. Chem. Soc., 2019, 141, 48, 19099-19109.
39. Mi-Hee. Jung, Inorganic Chemistry., **2019**, 58, 6748−6757.
40. L. Mao, Y. Wu, C. C. Stoumpos, B. Traore, C. Katan, J. Even, M. R. Wasielewski, M. G. Kanatzidis., Journal of the American Chemical Society., **2017**, 139, 11956−11963.
41. L. Mao, P. Guo, M. Kepenekian, I. Hadar, C. Katan, J. acky Even, R. D. Schaller, C.C. Stoumpos, and M.G. Kanatzidis, Journal of the American Chemical Society., **2018**, 140, 13078−13088.
42. M-H. Jung, Journal of Material Chemistry A., **2019**, 7,14689.
43. M. A. Haque, A. N. Gandi, R. Mohanraman, Y. Weng, B. Davaasuren, A-H. Emwas, C. Combe, D. Baran, A. Rothenberger, U. Schwingenschlögl, H. N. Alshareef, S. Dong, and T. Wu, Advanced Functional Materials., **2019**, 29, 1809166.
44. X. Liang, B. Li, M. H. Wang , J. Wang, R. L. Liu, and G. Li, ACS Applied Materials & Interfaces., **2017**, 9, 25082-25086.
45. L. Qin, Y-Z. Yu, P-Q. Liao, W. Xue, Z. Zheng, X-M. Chen, Y-Z. Zheng, Advanced Materials., **2016**, 28, 10772–10779.

View Article Online
DOI: 10.1039/D0TC01017K

COMMUNICATION

TOC

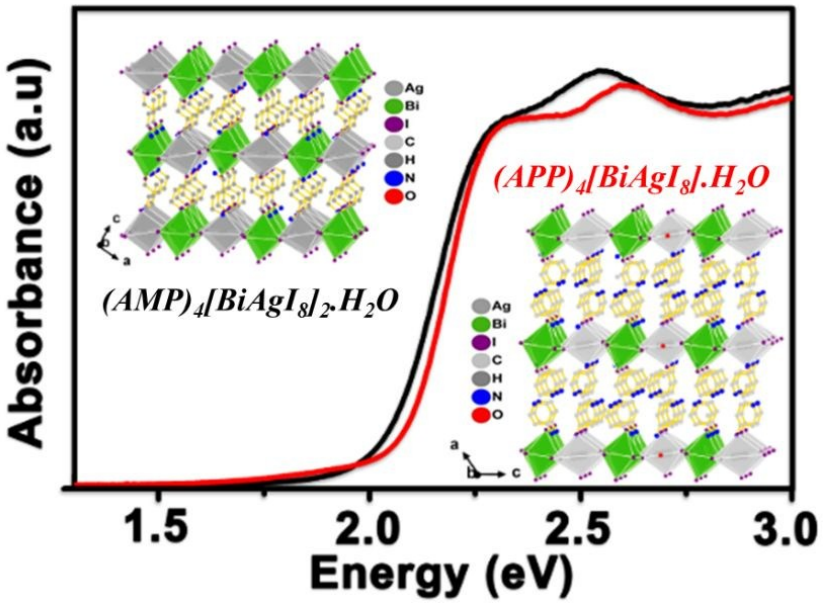

We report here two silver(I)-bismuth(III) based layered lead-free double perovskites with direct band gap and high moisture stability.